The Circularization of Amyloid Fibrils Formed by Apolipoprotein C-II

Danny M. Hatters,* Christopher A. MacRaild,* Rob Daniels,[†] Walraj S. Gosal,[‡] Neil H. Thomson,[‡]
Jonathan A. Jones,[§] Jason J. Davis,[¶] Cait E. MacPhee,[†] Christopher M. Dobson,[†‖] and Geoffrey J. Howlett*

*Department of Biochemistry and Molecular Biology, The University of Melbourne, Melbourne, Australia; [†]Cavendish Laboratory, University of Cambridge, Cambridge, United Kingdom; [‡]Astbury Centre for Structural Molecular Biology, University of Leeds, Leeds, United Kingdom; [§]Department of Physics, Clarendon Laboratory, University of Oxford, Oxford, United Kingdom; [¶]Inorganic Chemistry Laboratory, University of Oxford, Oxford, United Kingdom; and [‖]Department of Chemistry, University of Cambridge, Cambridge, United Kingdom

ABSTRACT   Amyloid fibrils have historically been characterized by diagnostic dye-binding assays, their fibrillar morphology, and a "cross-β" x-ray diffraction pattern. Whereas the latter demonstrates that amyloid fibrils have a common β-sheet core structure, they display a substantial degree of morphological variation. One striking example is the remarkable ability of human apolipoprotein C-II amyloid fibrils to circularize and form closed rings. Here we explore in detail the structure of apoC-II amyloid fibrils using electron microscopy, atomic force microscopy, and x-ray diffraction studies. Our results suggest a model for apoC-II fibrils as ribbons ~2.1-nm thick and 13-nm wide with a helical repeat distance of 53 nm $\pm$ 12 nm. We propose that the ribbons are highly flexible with a persistence length of 36 nm. We use these observed biophysical properties to model the apoC-II amyloid fibrils either as wormlike chains or using a random-walk approach, and confirm that the probability of ring formation is critically dependent on the fibril flexibility. More generally, the ability of apoC-II fibrils to form rings also highlights the degree to which the common cross-β superstructure can, as a function of the protein constituent, give rise to great variation in the physical properties of amyloid fibrils.

INTRODUCTION

Amyloid fibrils are protein aggregates most renowned for their association with neurological disorders such as Alzheimer's disease and Creutzfeldt-Jakob disease. Formation of fibrillar deposits by some 20 different proteins is associated with a number of both systemic and tissue-specific diseases (Sipe and Cohen, 2000). There appears to be little structural or sequence similarity between the functionally relevant forms of amyloid fibril-forming proteins; indeed, fibril formation appears to be favored by conditions under which the native structure of the protein is destabilized. In fact, it is now becoming evident that most, if not all, polypeptide sequences have the ability to form amyloid fibrils under appropriate in vitro conditions (Fandrich et al., 2001; MacPhee and Dobson, 2001).

Amyloid fibrils have traditionally been classified by their ability to interact with and alter the spectral properties of the dyes Congo Red and thioflavin T. These interactions are attributed to a common structural feature of all amyloid fibrils, namely the extensive β-sheet character of the peptide backbone. X-ray diffraction patterns of aligned amyloid fibrils indicate the presence of β-sheets that extend along the long axis of the fibrils and generate the core structure (Bonar et al., 1969). The fibril core is composed of at least two of these β-sheets spaced ~1.0–1.1-nm apart, giving rise to an architecture designated as cross-β (see Serpell, 2000, and references therein). These smallest core structures, often

described as protofilaments, range in width from 2.4 to 6 nm (Chamberlain et al., 2000), and in most instances mature amyloid fibrils are composed of several protofilaments which associate or intertwine, often to form a cable or ribbonlike morphology. It is at this level of assembly that substantial structural variation is seen among amyloid fibrils formed by different proteins or under different conditions. For example, analysis of several unrelated amyloid fibrils imaged by electron microscopy (Serpell et al., 2000) or by atomic force microscopy (Chamberlain et al., 2000) indicates fundamental differences in the footprint areas of the fibrillar cross sections. This variation has been interpreted as primarily arising from a variation in the number of protofilaments in the mature fibrils formed by different proteins (Serpell et al., 2000). There is also substantial variation in the structural arrangement of amyloid fibrils formed by individual proteins under different experimental conditions. For example, the fibrils formed by the SH3 domain of phosphatidylinositol-3′ kinase reveal a series of subtly different morphological forms, with the formation of flat ribbons, and also ropelike structures which show variations in the helical twist and the numbers of protofilaments that comprise the mature fibrils (Jimenez et al., 1999). In the case of the amyloid fibrils formed by islet amyloid polypeptide, sheetlike arrays appear to form through the side-by-side association of 5-nm-wide protofilaments (Goldsbury et al., 1997). Twisted ribbons also form through the lateral assembly of two, three, or five of the 5-nm protofilaments and cables are also formed by the intertwining of 8-nm-wide protofilaments. This wide variation of superstructural forms found within and between individual preparations of amyloid fibrils has significantly complicated attempts to elucidate the mechanisms of formation and the conformational behavior of amyloid fibrils.

Of all the amyloid fibril structures that have been observed to date, one particular example reveals an unusual variation on the assembly theme. Apolipoprotein C-II forms twisted ribbons including a minor proportion of structures in the form of closed loops (Hatters et al., 2000). In this current investigation, we examine the structure of amyloid fibrils formed by apolipoprotein C-II and probe the mechanism that allows the formation of closed rings. We examine two simple models for the generation of closed rings by apolipoprotein C-II fibrils and discuss the merits and limitations of each biophysical description.

MATERIALS AND METHODS

Protein preparation

ApoC-II was expressed (Wang et al., 1996) and purified as described previously (Hatters et al., 2000), with minor modifications. The washed inclusion bodies were dissolved in 50 mL of 5 M guanidine hydrochloride (GuHCl) and 100 mM arginine at pH 12.0, and applied in one loading to an XK 50-100 column packed in Sephadex G-75 pre-equilibrated with 6 M urea and 10 mM Tris-HCl at pH 8.0. The column was eluted at a flow rate of 2 mL/min with 6 M urea and 10 mM Tris-HCl at pH 8.0. The purity of the apoC-II protein eluted from anion exchange chromatography (Hatters et al., 2000) was deemed >95% as indicated by Tris-tricine SDS-PAGE (Schagger and von Jagow, 1987). ApoC-II was stored as a stock solution in 5 M GuHCl at a concentration of ~30 mg/mL. ApoC-II was diluted to 0.3 mg/mL in 0.1% (w/v) sodium azide and 100 mM sodium phosphate at pH 7.4. Amyloid fibrils were formed by incubation of the apoC-II solution at room temperature for two days.

X-ray fiber diffraction

A 1-mL solution of apoC-II fibrils was concentrated to ~200 μL using an Amicon YM-10 centricon (Millipore, Bedford, MA). 500 μL water was added and the sample re-concentrated to ~200 μl. This washing process was repeated twice more and the final volume was reduced to ~100 μL. The protein solution was dried from a droplet between two capillaries to form aligned fibrils as described in Serpell et al. (1999). The x-ray diffraction pattern of the fibrils was obtained using an 18-cm imaging plate detector (MarResearch, Norderstedt, Germany) with a Rigaku RU200 rotating anode (Rigaku USA, Danvers, MA).

Electron microscopy

Solutions of apoC-II were diluted threefold into 100 mM sodium phosphate, pH 7.4, and applied to freshly glow-discharged carbon-coated copper grids. The sample was washed once with water and negatively stained with 2% potassium phosphotungstate. The dried grids were imaged using a JEOL 2000FX transmission electron microscope (JEOL USA, Peabody, MA). The microscope was calibrated by photographing tobacco mosaic virus under the same conditions (Mandelkow and Holmes, 1974).

Atomic force microscopy

For ambient imaging, solutions of apoC-II fibrils were diluted 10-fold by the addition of 100 mM sodium phosphate buffer, pH 7.4, and applied to freshly cleaved mica (Agar Scientific, Cambridge, UK) and dried for several hours at room temperature. Imaging was performed using a MultiMode microscope (Digital Instruments, Ltd., Veeco Instruments, Watford, UK) in conjunction with a Nanoscope IIIa (Digital Istruments Ltd., Veeco Instru-

ments), control system as previously described (Chamberlain et al., 2000). The average diameter of the fibrils was determined by measuring cross-sectional heights at multiple arbitrary positions along the length of a number of fibrils. Ambient imaging was carried out with OTESPA-etched Si probes (Veeco Instruments), with a spring constant of 40–50 N/m, at resonant frequencies of 250–400 kHz. For imaging under fluid, a freshly prepared solution of poly-L-lysine (0.1% w/v in water (Sigma, St. Louis, MO)) was applied to freshly cleaved mica for 1 min. The mica was then thoroughly rinsed, first in water, and then in 100 mM sodium phosphate buffer, pH 7.4. Solutions of apoC-II fibrils were diluted 10-fold into 100 mM sodium phosphate buffer, pH 7.4, and applied to the mica for several minutes before thorough but gentle rinsing with 1–2 mL of 100 mM sodium phosphate, pH 7.4. The mica was immediately placed into a Digital Instruments fluid cell without the O-ring. Imaging under fluid was carried out using tapping mode atomic force microscopy (AFM) using silicon nitride probes with a spring constant of 0.12 N/m. The sample under study was immersed in 100 mM sodium phosphate solution, pH 7.4, as described previously (Chamberlain et al., 2000).

Image analysis

Electron micrograph negatives were digitized using an Epson GT-7000 USB scanner (Epson, Southbank, Victoria, Australia) with a film adaptor. Helical repeat, and contour length measurements (L) were recorded on the digitized images using the software package ScionImage (Scion Corporation, Frederick, MD). Contour lengths were measured on isolated fibrils using the tracing tool with the corresponding end-to-end distances calculated using the line tool. The distance units were calibrated using the scale bar on the electron micrographs.

THEORY

Persistence length estimations from two-dimensional images

The persistence length of apoC-II amyloid fibrils in solution was estimated from conformational parameters measured by electron microscopy. During deposition onto the electron microscope (EM) grid, the three-dimensional solution conformation of amyloid is inevitably altered by the transformation onto a two-dimensional surface. For this deposition process, fibrils can either conformationally equilibrate as they settle or directly adhere to the surface through grid-fibril attractive forces. The mean-square end-to-end distance of a fibril of contour length L and persistence length P assuming conformational equilibrium in two dimensions is given by Rivetti et al. (1996),

$$\langle R^2 \rangle_{2D} = 4PL \left(1 - \frac{2P}{L} \left(1 - e^{-L/2P} \right) \right). \qquad (1)$$

The observed conformation of the amyloid fibrils is assumed to be the result of flexibility, rather than reflecting an inherently bent structure. This assumption appears to be validated by the alignment of fibrils as demonstrated by x-ray diffraction.

Random walk model

For ease of use we assume a Gaussian distribution (Doi and Edwards, 1986; De Gennes, 1985) for the end-to-end vector,

and work in three dimensions. Going beyond this Gaussian approximation would prove to be very difficult analytically (Doi and Edwards, 1986; De Gennes, 1985), and would unnecessarily obscure the underlying physics. The length L of the chain is given by $L = Nb$, where N is the number of steps, and b is the step-length. Any flexible (or semiflexible) chain can be approximately modeled in this way, provided we use an appropriate value for the step-length b.

In our approximation, the probability $P(\Delta \vec{R}, N)$, that the end-to-end vector of a Gaussian chain consisting of N links is $\Delta \vec{R}$, is given by Doi and Edwards (1986) and De Gennes (1985), as

$$P(\Delta \vec{R}, N) = \left(\frac{2\pi \langle R^2 \rangle}{3} \right)^{-3/2} \exp\left(-\frac{3(\Delta R)^2}{2\langle R^2 \rangle} \right). \quad (2)$$

Note that $P(\Delta \vec{R}, N)$ is normalized such that $\int d^3 \Delta R P(\Delta \vec{R}, N) = 1$, and $\int d^3 \Delta R P(\Delta \vec{R}, N)(\Delta R)^2 = \langle R^2 \rangle$.

We are interested in calculating the probability of closed loop formation, $P(0, N)$. We can obtain this distribution straightforwardly by setting $\Delta \vec{R} = 0$ in Eq. 2. We then obtain an approximate expression for the probability of loop formation as

$$P(\Delta \vec{R}, N) = \left(\frac{2\pi \langle R^2 \rangle}{3} \right)^{-3/2}. \quad (3)$$

For an ideally flexible chain (in any dimension), the relation $\langle R^2 \rangle \sim N$ holds (Doi and Edwards, 1986; De Gennes, 1985).

Chain stiffness considerations

The effects of stiffness are twofold.

Firstly, for a freely-jointed chain (in three dimensions), the ideal result for $\langle R^2 \rangle$ given above is modified to (Rivetti et al., 1996; Doi and Edwards, 1986; De Gennes, 1985)

$$\langle R^2 \rangle = b^2 \left[N \frac{1 + \cos \alpha}{1 - \cos \alpha} - 2 \frac{\cos \alpha}{(1 - \cos \alpha)^2}(1 - \cos^N \alpha) \right]. \quad (4)$$

In this approach, we model inherent chain stiffness by assuming that the angle between consecutive bond vectors is given by the fixed value α. We can also make the following correspondence in the large-length limit. Using the relation

$$L = Nb \quad (5)$$

for consistency, we must identify

$$b = 2P \frac{1 - \cos \alpha}{1 + \cos \alpha}. \quad (6)$$

Secondly, stiffness imposes the condition that the probability for the formation of loops is strictly zero for random walks with a number of links N less than some minimum value $N_{\min}$. This intuitively reflects the fact that we require a minimum number of straight, rigid line elements to form

a single loop, given a fixed angle between bond vectors. Any loops with a number of straight steps N less than $N_{\min}$ are ruled out on physical grounds, due to the effect of high curvature penalization. The condition for loop formation can be expressed as

$$N_{\min} \geq \frac{2\pi}{\alpha}. \quad (7)$$

Using Eq. 4, $N_{\min} b = L_{\min}$, and Eq. 5 and Eq. 6, we can calculate $N_{\min}$, α, and b, given the values of P and $L_{\min}$.

Incorporating both of the above effects of stiffness on our chain, our final approximate expression for the probability distribution of fibril loop formation looks like

$$P(\Delta \vec{R}, N) = 0 \quad \text{for } N < N_{\min},$$

$$P(\Delta \vec{R}, N) = \left(\frac{2\pi \langle R^2 \rangle}{3} \right)^{-3/2} \quad \text{for } N \geq N_{\min}, \quad (8)$$

with $\langle R^2 \rangle$ given by Eq. 3.

Monte Carlo simulations

A wormlike chain model of loop closure probability was explored using Monte Carlo simulations based on methods developed for the problem of DNA cyclization (Levene and Crothers, 1986; Kahn and Crothers, 1998). Fibrils are simulated as chains of n segments, each of length $l = 10$ nm and infinitesimal thickness. Computationally, each chain segment is taken as a unit vector along the z-axis of a local coordinate frame. The z-axis of this frame thus represents the fiber axis, while the y-axis is taken as the normal to the plane of the fibril ribbon and the x-axis parallel to the amyloid β-strands. The orientation of each segment in the coordinate frame of the previous one is defined by three angles, θ, ϕ, and τ, which correspond to rotations about the x-, y-, and z-axes, respectively. Thus θ represents bend perpendicular to the plane of the amyloid ribbon, ϕ represents bend in the plane of the ribbon, and τ represents twist along the fiber axis. The full trajectory of each chain is defined by expressing the coordinates of chain segments 2–n in the frame of the first chain element.

The values of θ, ϕ, and τ at each joint of the chain are determined as normally distributed pseudo-random numbers with standard deviation, σ, about a mean for each angle. We have set the mean values for θ and ϕ to 0, reflecting the assumption that observed curvature reflects fibril flexibility and not an intrinsic bend. We have also assumed negligible bending in the plane of the amyloid ribbon, thus $\sigma_\phi = 0$, allowing σ_ϕ to be determined from the relation (Levene and Crothers, 1986) of

$$\sigma_\theta^2 + \sigma_\phi^2 = \frac{2l}{P}. \quad (9)$$

The mean and standard deviation of τ was determined from EM data by measuring the length of helical repeat distances

in the amyloid fibrils. For each of 20 chain lengths in the range 40 nm to 10 μm ($n = 4$ to $n = 1000$) we generated a data set consisting of $\sim 10^9$ chains. For computational efficiency N chains are generated at half of the desired length, and then joined pair-wise, end-to-end, to yield the final data set of N^2 chains.

An estimate of loop closure probability is derived from each data set by determining the proportion of chains in the set which have ends in an appropriate orientation with respect to each other to allow annealing. Specifically, to be considered a potential loop, chains must meet three conditions. Firstly, the end-to-end distance, R, must be less than some tolerance, R_{tol},

$$R \leq R_{tol}. \qquad (10)$$

Secondly, the tangents to the chain at each end must align to within a tolerance Ω_{tol}. This is constrained by

$$\sqrt{\Theta^2 + \Phi^2} \leq \Omega_{tol}, \qquad (11)$$

where Θ and Φ are the in-plane and out-of-plane bend angles of the last chain segment, expressed relative to the first chain segment. Finally the helical twists of the fibrils must be in register,

$$T \leq T_{tol}, \qquad (12)$$

where T is the twist of the last segment relative to the first. To obtain continuous functions relating loop closure probability to chain length at each persistence length, the results from the simulations were interpolated using Akima splines. In relating fibril contour length to aggregation number we have assumed a linear density of 1 apoC-II molecule per nm.

RESULTS AND DISCUSSION

Amyloid fibril core structure

Fig. 1 shows an electron micrograph of apoC-II amyloid fibrils demonstrating the presence of long, tangled twisted ribbons and shorter closed loops. X-ray diffraction techniques were used to probe further the secondary and tertiary structures of these fibrils. The pattern of diffraction (Fig. 2) indicates reflections corresponding to a meridonal distance of 0.47 nm and equatorial distance of 0.94 nm. This diffraction pattern is characteristic of the typical cross-β structure of amyloid fibrils (Serpell et al., 1999) and indicates the presence of at least two β-sheets assembled along the fibril axis, with the β-strands perpendicular to the long fiber axis.

We further probed the structure of the amyloid fibrils using AFM, which allows topographical data of amyloid fibrils to be recorded directly—revealing, in particular, the height of the fibrils when laid down on a substrate surface. Images were initially recorded of fibrils dried onto mica (Fig. 3 a). The fibrils have a similar tangled appearance to those imaged by negative staining electron microscopy
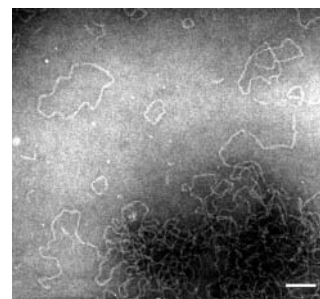

FIGURE 1 Negatively stained transmission electron micrograph of a sample of apoC-II fibrils showing extended structures and closed loops. Samples were stained with 2% (w/v) potassium phosphotungstate and show semiregular helically twisted ribbons. Scale bar represents 100 nm.

(Fig. 1), providing confidence that the morphology is intrinsic to the sample rather than arising from the preparation of the samples for imaging. Fibrils were also imaged in the presence of sodium phosphate buffer by in situ AFM. Fibrils could not be imaged directly on mica in the presence of buffer, since the fibrils did not remain fixed to the surface causing interference with the imaging. Instead, the fibrils were attached to the substrate via electrostatic interactions with poly-L-lysine-coated mica. Imaging of fibrils prepared this way revealed a morphology similar to that of apoC-II fibrils dried onto mica (Fig. 3 b). Importantly, imaging of both dried apoC-II fibrils and of fibrils in refolding buffer revealed the presence of closed loops, indicating specifically that the loops are not an artifact of the drying or staining processes peculiar to electron microscopy (Fig. 3 c). The fibrils proved fragile in aqueous buffer as indicated by the existence of significant fragmentation in images acquired over multiple scans (Fig. 3 d). The breakage was most sensitive at the bends of the fibrils, perhaps as a result of torsional stress resulting from strong adherence of the negatively charged amyloid fibrils onto the positively charged poly-L-lysine coating the mica. This fragmentation of the fibrils in solution made the recording of high-
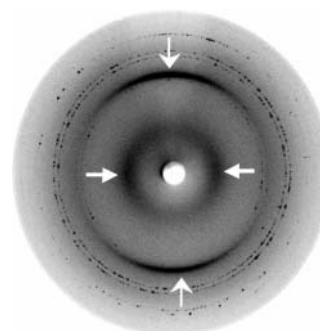

FIGURE 2 X-ray diffraction pattern of aligned apoC-II fibrils. Vertical arrows point to strong meridonal reflections at 0.47 nm and the horizontal arrows point to equatorial diffraction patterns at 0.94 nm. The outer sharper rings represent reflections resulting from residual salts in the buffer.
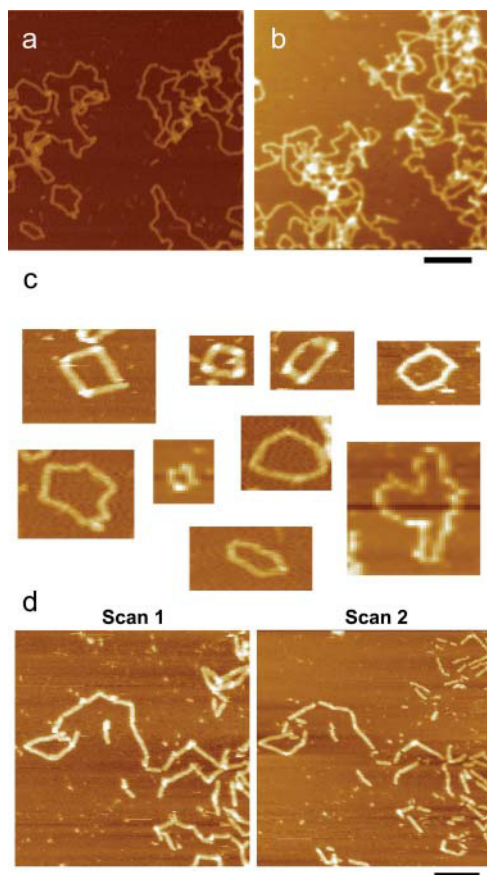
FIGURE 3 Atomic force micrographs of apoC-II amyloid fibrils. Samples of apoC-II fibrils were imaged either directly in buffer (100 mM sodium phosphate, pH 7.4) on poly-L-lysine-coated mica (*a*) or dried directly onto mica (*b*). Scale bars for *A*, *B*, and *D* represent 100 nm. A montage of selected loops is shown in *c*. Example of fibril fragmentation of fibrils imaged in buffer with the first scan (*left*) and the subsequent scan (*right*) highlighting points of fragmentation (*d*).

resolution images difficult. For this reason, subsequent AFM analysis was focused on the study of the amyloid fibrils dried onto mica.

A contour map of an apoC-II fibril imaged in air and on mica is shown in Fig. 4. This image demonstrates the regular undulation in the height of the fibrils as represented by alternating peaks and dips along the axes of the fibril (Fig. 4). This alternation is consistent with a twisting around of the helical ribbon morphology that is apparent in the electron micrographs (Fig. 1). Analysis of the height data for a number of fibrils reveals a modal ribbon height for the dried fibrils of 2.1 nm (Fig. 5), with a minimum height of 1.3 nm and a maximum height of ~3.2 nm. In solution, the measured fibril diameter was slightly larger (3.5 nm), suggesting some compression of the fibrils on drying onto the surface. It is interesting to compare these data with the heights of other amyloid structures measured by AFM in air and in solution. For example, a mean thickness of 4.4 nm has been measured under fluid for the cylindrical amyloid fibrils formed by a peptide (residues 10–19) of transthyretin and a thickness of

7.8 nm reported for amyloid fibrils composed of four protofilaments formed from an SH3 domain (Chamberlain et al., 2000). Amyloid fibrils of α-synuclein have an average thickness of 7.6 nm at the highest point along the helical twist of the fibril as measured using tapping-mode AFM in air (Rochet et al., 2000). Tapping-mode AFM does not necessarily always measure true heights in air or under fluid, due to the complex mechanisms of contrast generation, which makes exact comparisons between different systems and imaging conditions difficult. Nevertheless, the thickness observed here for apoC-II fibrils is more comparable to the thickness observed for protofilaments of other amyloid fibrils, suggesting that the apoC-II fibrils have a relatively simple structure. Moreover, a thickness of 2.1 nm is compatible with two β-sheets stacked together, taking into consideration the intersheet distance of ~1 nm and allowing for the distance of the side chains extending from each external side of the β-sheets (~0.5 nm per β-sheet). Indeed, this dimension is close to the thickness of the individual SH3 protofilaments that have previously been modeled in detail on a pair of β-sheets (Jimenez et al., 1999). The diffuse equatorial reflections in the x-ray data are also consistent with a core of only two β-sheets, inasmuch as these reflections become more coherent with increasing numbers of sheets.

We have developed one possible model for the assembly of apoC-II into fibrillar ribbons composed of two β-sheets that run along the fibril axis, separated by ~0.94 nm. The arrangement of the β-sheets is derived from three sets of data: the x-ray diffraction data which indicate cross-β structure; the cross-sectional size of the fibrils derived from the electron microscopy data, suggesting a width of 12 nm; and the AFM data suggesting a thickness of ~2.1 nm. Although the maximum height of the fibrils measured by AFM (~3 nm) is significantly smaller than the 12-nm ribbon width observed by transmission electron microscope, we suggest that the AFM thickness arises from compression of the dried sample on the surface. In our model, the simplest monomer conformation within the fibril would be a single hairpin, giving rise to a ribbon width of 12 nm. The hairpin may have the conventional β-hairpin configuration, in which the two strands are connected by intramolecular hydrogen bonds and form part of the same sheet. Alternatively, the apoC-II polypeptide chain might adopt an intramolecular β-sheet conformation, as proposed by Pham et al. (2002). A similar structural model was originally suggested for the Aβ peptide by Tjernberg et al. (1999) and has been further elaborated more recently by Petkova et al. (2002). In this model, the two strands of the hairpin are in separate β-sheets and make contacts through favorable side-chain interactions. Either of these conformations fulfill the basic requirements of cross-β structure and match the expected apoC-II hairpin length of 11.5 nm. Even though a β-strand of 12 nm is unusually long, it is not unprecedented in length. For example, a β-strand of 9.3 nm in length is observed in the
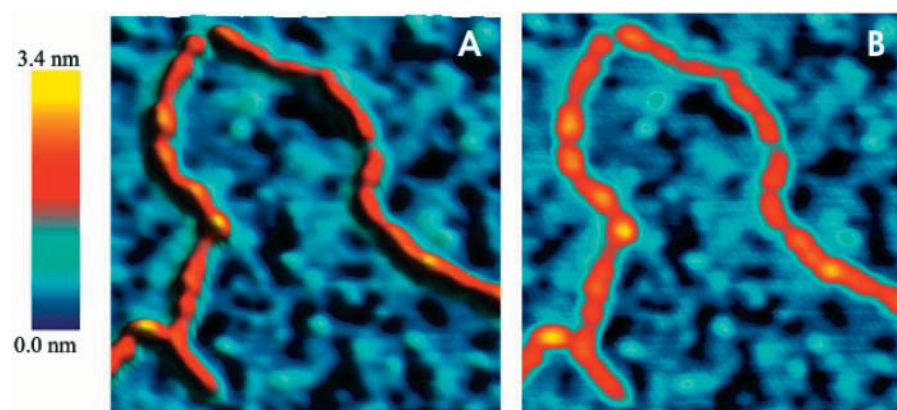
FIGURE 4 Tapping-mode AFM image of an apoC-II fibril dried onto mica. *A* is a pseudo-three-dimensional representation of the data, which highlights the undulations along the fibril backbone, whereas *B* is a conventional false-color image representation of the AFM height data. The height ranges from 0 nm (*dark blue*), the mica background, to 3.4 nm (*yellow*), the peak heights on the fibril. As well as the bound fibrils, there is a background consisting of buffer salts, monomeric apoC-II, and possibly oligomeric species. This forms a smooth layer of ~0.5 nm and is interspersed with a network of holes down to the mica surface.

crystal structure of proaerolysin (Parker et al., 1994). However, the small size of protofilaments observed in other amyloid systems (<6 nm; Chamberlain et al., 2000) suggests that the apoC-II ribbon may be composed of at least two β-strands. There was no evidence of fibrils splitting into protofilament substrands in the AFM data such as those observed with wild-type lysozyme amyloid fibrils, which could mean that if they do exist, they are too small to be imaged or are unstable and rapidly disintegrate. Our model implies that the ends are the reactive species in amyloid fibril growth. This raises the possibility of loop formation occurring through the adherence of one end of a fibril to the other.

Analysis of fibril flexibility

The twisted and tangled nature of the structures imaged by EM and AFM (Figs. 1 and 3) could be explained by the existence of flexibility within the apoC-II amyloid fibrils. Moreover, the ability to form loops suggests that fibrils are able to explore a range of different structures, some of
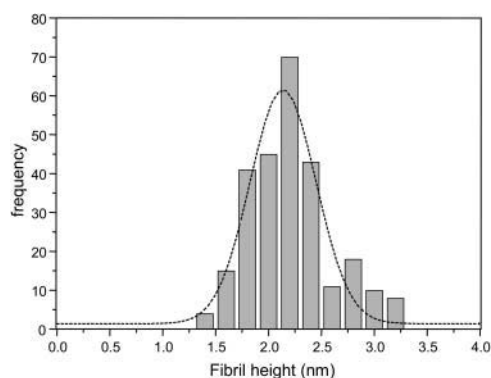

FIGURE 5 Histogram of height data recorded from atomic force micrographs of dried apoC-II fibrils. The data shown are differences between the maximum heights on cross sections perpendicular to the fibril long axis (i.e., fibril backbone) and the mica baseline (excluding salt, monomeric, or oligomeric species bound in the background).

which might then persist once formed. On this assumption, we have explored two highly simplified models based on a flexible ribbon having a certain probability of loop closure. The models require defining the persistence length of the structure, data for which were obtained from digitized electron micrographs by measuring contour lengths and corresponding end-to-end distances of apoC-II fibrils that were not evidently in closed loops. If it is assumed that the fibrils reach conformational equilibrium as they settle onto the EM grid, the relationship between the contour length and the mean-square end-to-end distance is given in Eq. 1 (Rivetti et al., 1996). Where only weak interactions exist between the two-dimensional surface and fibrils, conformational equilibrium is attained before deposition. This is highlighted by studies on the deposition of individual DNA molecules onto mica, where conformational equilibrium is reached on nonadhesive surfaces, compared to deposition in kinetically trapped conformations on surfaces for which they have greater affinity (Rivetti et al., 1996). We make the assumption that apoC-II amyloid fibrils have minimal affinity with the EM grid and therefore equilibrate on that surface during deposition. This assumption is supported by the observation that fibrils are easily washed entirely off the grid. On the other hand, the fragility of the fibrils on poly-L-lysine-treated silica suggests a more strained kinetically trapped conformation. Fits of contour length versus the square of the end-to-end distance to Eq. 1 yield a persistence length of apoC-II amyloid fibrils of 36 nm (Fig. 6). These results can be compared to a persistence length of 53 nm measured for DNA imaged by AFM using the same conformational assumptions (Rivetti et al., 1996).

The helical repeat distances were measured from electron micrographs, where the helical repeat was determined as the distance between the midpoints of two consecutive narrow segments of low density within an amyloid fibril (Fig. 1). This corresponds to sections in which the amyloid ribbon lies perpendicular to the surface. The helical repeat thus represents a 180° twist in the amyloid ribbon. A histogram of the helical repeat lengths and the fit of the data to a normal distribution are shown in Fig. 7. The fitted distribution
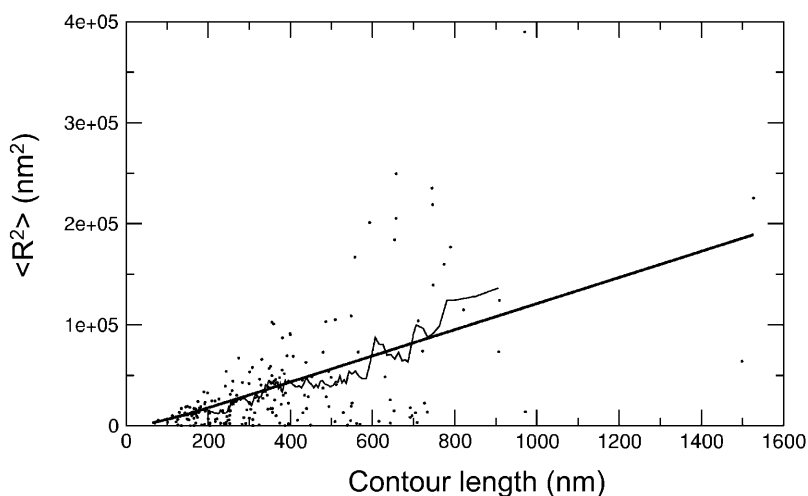
FIGURE 6 Interpretation of the persistence length of apoC-II amyloid fibrils. Squared end-to-end distances versus contour lengths of amyloid fibrils as measured from electron micrographs are plotted as dots. The data fit to Eq. 1 for a model describing the persistence length of fibrils in an equilibrated two-dimensional conformation is represented as a heavy line. A running average of the end-to-end distances of the fibrils of a window size of 15 (*thin solid line*) is shown as a comparison with the fit to the model describing persistence length.

reveals a mean helical repeat length of 53 nm and a standard deviation of 12 nm. This represents an average helical twist of 3.4°/1 nm of fibril, which compares to a twist of 2.9–3.1°/nm for the model developed for SH3 domain amyloid fibrils (Jimenez et al., 1999).

Kinetic considerations

Any attempt to understand the physical basis of loop formation will necessarily include a consideration of the kinetics of fibril elongation, conformational resampling and loop closure; furthermore, the observation that apoC-II amyloid fibrils are able to form closed loops sheds some light on the timescales of fibril growth and conformational dynamics. In the event that either fibril elongation or conformational relaxation occur much faster than the reaction by which loops are closed, no loops will be formed because no fibril will exist in a conformation and length suitable for loop formation for sufficient time for the loop-closure reaction to occur. Thus the existence of loops implies
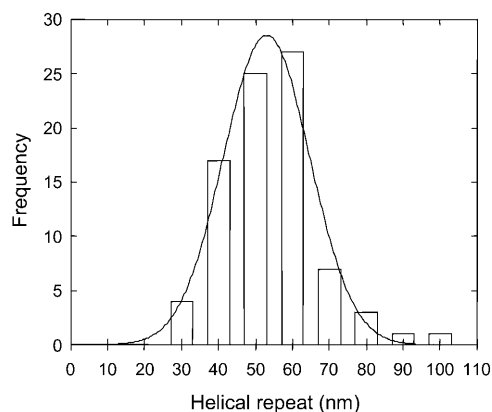

FIGURE 7 Histogram of the helical repeat distances of apoC-II fibrils. The data were fitted to a normal distribution (*solid line*) yielding a mean of 53 nm and a standard deviation of 12 nm.

that the rate of loop closure for apoC-II fibrils is of similar order to, or greater than, the rates of fibril elongation and fibril conformational change. On the other hand, if fibril elongation is much slower than conformational sampling and loop closure, each fibril will spend sufficient time at some minimum loop-forming length to find a loop-competent conformation and anneal. In this case we would expect all fibrils to form loops of approximately equal size. Examination of Figs. 1 and 3 reveals loops of a broad range of sizes, as well as a large number of very long fibrils that do not appear to have formed loops. Although precise quantification is not possible due to the highly entangled appearance of the longer fibrils, we estimate that <10% of all fibrils present are loops. Clearly then, we must exclude kinetic schemes in which apoC-II fibril elongation is significantly slower than conformational dynamics or loop closure.

To understand this somewhat counterintuitive finding we must consider the kinetics of amyloid fibril formation in some detail. This has been particularly well studied in the case of the Alzheimer's associated Aβ-amyloid fibrils, and from this and other work involving cytoskeletal fibrils a general model of fibrillar protein polymerization has been developed (Ferrone, 1999). The fibril architecture of apoC-II amyloid appears to be simple with no evidence of protofibrils existing separately as precursors to amyloid ribbons and with a strikingly homogeneous morphology compared to other amyloid systems. On this basis we ignore the fibril-fibril interactions and protofilament aggregation that are important factors in the Aβ kinetic scheme (Goldsbury et al., 1997; Jimenez et al., 1999; Chamberlain et al., 2000). In general, fibrils are thought to assemble by a nucleation-dependent polymerization mechanism akin to protein crystallization phenomena, involving a slow transition through a highly unstable nucleus which is presumed to be some form of small prefibrillar aggregate (Lomakin et al., 1997). Fibril elongation proceeds by means of addition of monomers or possibly small oligomers to the growing ends of the fibril. Support for this mechanism arises from the observation that the addition

of preformed fibrils promotes fibril elongation (e.g., Come et al., 1993). In the case of apoC-II we have previously demonstrated that, after nucleation, fibril elongation is rapid—with the lack of populated intermediates in the elongation pathway indicating a timescale of a few minutes or less for the full transition from the nucleating species to mature fibrils many microns in length (Hatters et al., 2001; MacRaild et al., 2003). Because this transition encompasses many thousands of molecular addition events, the underlying molecular rates are probably no slower than tens of milliseconds. On the other hand, nucleation typically proceeds over several days under the conditions relevant to the present study and is the rate-limiting event in the aggregation process (Hatters et al., 2001).

The conformational dynamics of amyloid fibrils are more poorly understood, and have been addressed in detail only in the case of gels formed by synthetic amyloid-like fibrils (Aggeli et al., 1997; Gosal et al., 2002). For such systems conformational relaxation times are outside the range addressed by rheological measurements, being longer than tens of seconds (Aggeli et al., 1997). In the case of the more dilute fibril solutions studied here, conformational relaxation can be expected to be faster due to the reduced number of fibril entanglements. Such entanglements do persist in apoC-II fibril solutions down to low concentrations; however, MacRaild et al. (2003) and recent measurements suggest conformational relaxation times for apoC-II fibrils at 0.3 mg/mL as long as hundreds of ms (MacRaild et al., in preparation).

The foregoing discussion of the kinetics of amyloid formation implies that the concentration of monomeric apoC-II in solution is effectively constant during the growth of any given fibril. We make the assumption that fibril elongation rates are independent of fibril length over the range of lengths for which they are competent to form loops. This assumption can be justified on the basis that the observed loop species appear significantly smaller than other fibrils, suggesting that loops are not formed by fibrils near their maximum length. It is also significant to note that growth of preformed fibrils of $A\beta$ occurs at a rate first-order in monomer concentration with no apparent length dependence (Naiki and Nakakuki, 1996). A further assumption is that loops are stable once formed, with only the fibril ends susceptible to growth or degradation. This assumption is supported by the absence of short linear fibrils and by the observation that the number of loops is not reduced in samples incubated for periods as long as several months. From these considerations it is apparent that any growing fibril will spend equal time at each of the loop-competent lengths. Furthermore the previously noted observation that a large majority of fibrils grow to very long lengths and do not form loops indicates that at any time the population of growing fibrils is not substantially depleted by the formation of loops. Given this, the probability that any fibril will form a loop of a given length will be proportional to the probability of that loop being in a loop-competent conformation at a single instant of time. By extension it can be seen that the observed distribution of loop sizes will be identical in shape to the probability distribution of loop closure with respect to fibril length.

Loop closure probabilities

Two models are typically employed to describe the elastic behavior of polymer chains: the random walk and the wormlike chain. In the first, each segment of the polymer is independent of the next, and a path is constructed on a lattice where the choice of direction for each step is limited and the step length is fixed. Loop formation occurs when the paths of the two ends coincide on the lattice. In the second, a wormlike chain is treated as a stiff rod, within which the length over which the memory of the initial orientation of the chain persists (the persistence length) defines the stiffness of the chain. Fibril annealing is inferred when the ends of the polymer chain fulfill certain loop closure criteria defined by physical tolerances. Although theory describing polymer cyclization processes based on the former model is well established (Jacobson and Stockmayer, 1950), extension of this approach to the more general latter case of constrained wormlike chains has not been achieved. Herein, we employ both models to describe the behavior of amyloid fibrils assembled from apoC-II.

Random walk model

The random walk description is an approximate one, but possesses two important qualities: firstly, it renders the underlying physics of fibril loop formation transparent; and secondly, the model given below agrees with an intuitive explanation for the observation of fibril loops. This explanation can be crudely stated as follows. The formation of small loops is energetically unfavorable due to the steric strain of short length fibrils bending back on themselves sufficiently for loop closure. In contrast, the ends of long-length fibrils will not be able to find each other in three-dimensional space, and so large loops are also suppressed. Somewhere in between these very short and very long fibril length-scales, conditions are most favorable for loop creation and we will observe a single peak in a loop probability distribution. Shown in Fig. 8 A is a comparison of the experimentally observed loop probability distribution, and the theoretical loop probability distribution for amyloid fibrils given by Eq. 8.

Experimentally it was found that the persistence length is given by $P = 36$ nm. From the experimental data in Fig. 8, we determine $L_{\min} = 205$ nm. Given these values, and using Eqs. 5–7, we get

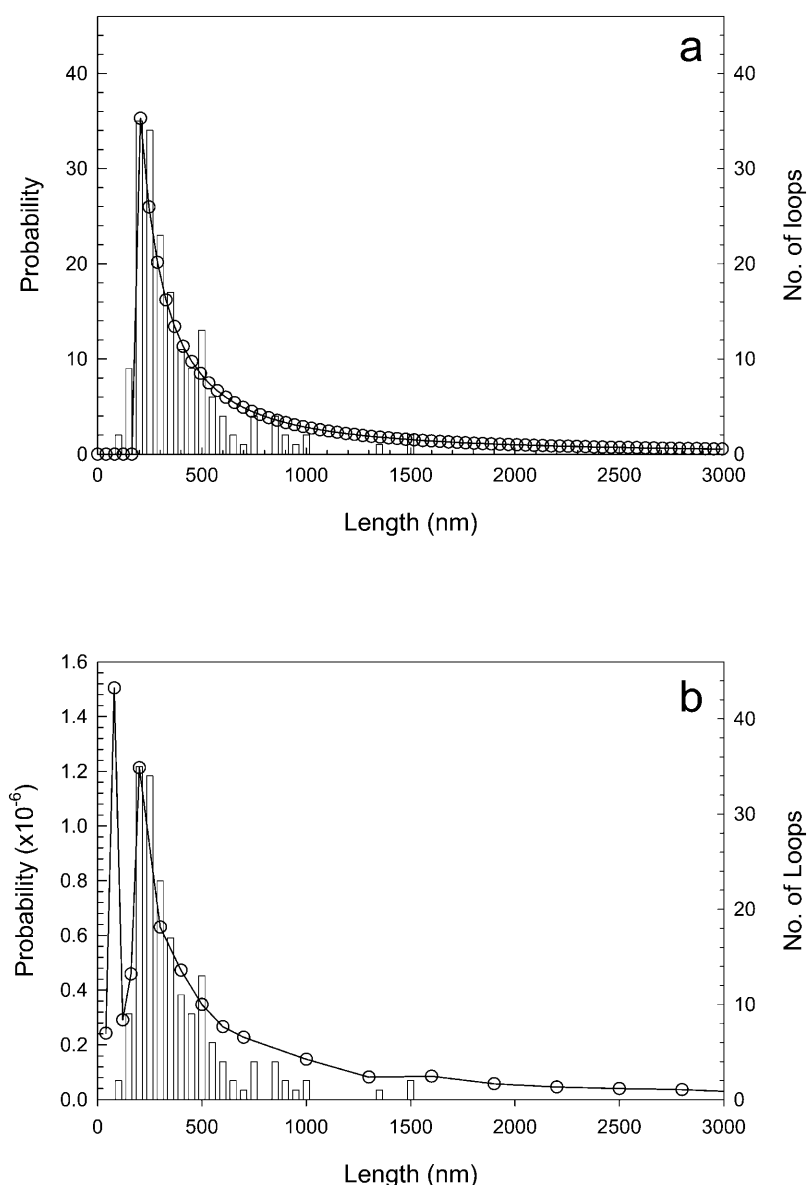$$N_{\min} = 5, \quad \alpha = 0.8\frac{\pi}{2}, \quad \text{and} \quad b = 41 \text{ nm}.$$

FIGURE 8   Loop closure probabilities as predicted using the random walk (*a*), or the wormlike chain (*b*), models of fibril behavior. The left axes represent loop closure probabilities determined from the models whereas the right axes represent the size distribution of loops as measured from digitized electron micrographs. The probability function generated by the random walk model *a* is described by Eq. 8. The loop closure probability function calculated from the wormlike chain model *b* was determined from 20 Monte Carlo simulations using conditions for loop closure determined from Eqs. 10–12, where $R_{tol} = 5$ nm, $\Omega_{tol} = 0.5$ rad, and $T_{tol} = 0.79$ rad, and the chains were generated using a persistence length of 36 nm. The total number of chains in each simulation was 10^9.

The position of the peak in the loop probability distribution function versus chain length depends on the stiffness of the chains. This is consistent with the intuitive idea that stiffer chains will be less successful than more flexible chains at forming shorter length loops, whereas the longer the chain, the less successful it will be at forming loops due to the larger number of configurations available to it. This is evident in the slowly decaying tail of the loop probability distribution of Fig. 8 *A*. However, from the data we see that the random walk model overpredicts the number of loops formed at large length scales, implying that our simple and approximate semiflexible random walk model does not accurately capture the conformational properties of very long amyloid fibrils. This could be due to the lack of an explicit self-avoidance constraint (Doi and Edwards, 1986; De Gennes, 1985) in our model. Alternatively, there might exist subtle physical

reasons why too few large length loops are detected experimentally. For example, it is possible that the extensive tangling of these species impedes their identification by electron microscopy. We have also assumed in this work that the effects of intrinsic chain twist on the probability distribution for loop formation can be safely ignored. This question of whether the ends of a fibril need, not only to come close enough together to form loops, but also to be aligned correctly in physical space, is addressed by modeling of the amyloid fibril as a wormlike chain.

Wormlike chain model

A wormlike chain model of loop closure probability was explored using a Monte Carlo simulation approach based on those previously developed to describe DNA circularization

(Levene and Crothers, 1986; Kahn and Crothers, 1998). Initially we create wormlike chains to simulate amyloid fibrils with a persistence length of 36 nm and an average helical twist of 0.59 rad per 10-nm chain segment (Fig. 7). Sets of chain conformations were then assessed for potential loop closure on the basis of the conditions defined in Eqs. 10–12. A distribution function was generated describing an empirical relation between loop closure probability and chain length, employing tolerance values of 5 nm for the permitted tolerance in the end-to-end distance (R_{tol}), 0.5 rad for the tolerance in the chain alignment (Ω_{tol}), and 0.79 rad for the permitted variation in the alignment of the ribbon twist (T_{tol}). These values are selected on the basis of the resolution of the model, which is dictated by the 10-nm chain segment length. Comparison between the experimentally observed and theoretically calculated probabilities of loop formation is shown in Fig. 8 *B*. At small chain lengths the probability of loop closure is zero, but rises rapidly with increasing chain length, to double maxima at 80 and 200 nm. After the second maximum the probability function decays to vanishing probabilities. Given that the average length of a full twist is ~106 nm, the two maxima most likely arise as a result of a requirement for twist alignment.

The influence of the tolerance values R_{tol}, Ω_{tol}, and T_{tol} on the probability of loop closure within the simulation was explored by systematic variation of these parameters. As expected, the probability of the formation of closed loops decreases as each tolerance is made more stringent. It must be noted, however, that we do not attempt to interpret the magnitude of the probability function, as to do so would require a complete understanding of the kinetics of both fibril growth and loop closure (see the previous discussion of kinetic considerations). Instead we are interested only in the shape of the probability function with respect to fibril length, as this shape is expected to match the observed distribution of loop lengths. The shape of the probability function shows no significant dependence on R_{tol} or T_{tol}, indicating that the value chosen for these parameters has no impact on our findings here. The same is true of Ω_{tol}, except in the case of very short fibril lengths $<$~150 nm. At these lengths the probability of loop closure is disproportionately reduced by increased stringency in Ω_{tol}. In the current context, the effect of this is to reduce the relative amplitude of the 80-nm probability maximum compared to the 200-nm maximum as Ω_{tol} is reduced. This may be rationalized by noting that owing to the ribbonlike nature of the fibrils, short fibrils are unlikely to exist with their ends close together and in tangential alignment.

Two points of difference between the probability function and the observed distribution can be noted: short chain length loops corresponding to the first maxima observed in the probability function are not observed experimentally; and the incidence of loops observed experimentally decreases more rapidly with chain lengths $>$600 nm compared to the simulated probability function. As indicated above, the

disagreement at longer chain lengths could be due to tangling of longer chains and the consequent difficulty in identification of longer loops in the electron micrographs. The former discrepancy—the observation of a peak in the probability distribution at 80 nm—is most likely an artifact of the sharp dependence of the shorter probability maximum on Ω_{tol}. The loops predicted at 80 nm represent a 360° twist of the fibril ribbon, and should therefore be ~106 nm in length (Fig. 7). The length of this 360° twisted loop is reduced to 80 nm due to the fact that by selecting for small loops with their ends close enough to anneal, and with their chain alignments (Ω_{tol}) within the tolerances, the twist alignment must, with very high probability, also fall within the tolerances. This peak therefore represents an artificial selection for the extremes of physical behavior: i.e., those fibrils displaying the shortest possible twist repeat length and the greatest possible curvature. Visual examination of a selection of simulated loops falling within this peak indicates that loops of this size, with the fibril dimensions of the apoC-II amyloid ribbon, would suffer extensive fibril-fibril overlap. On this basis we suggest that steric effects account for the fact that these loops are not observed experimentally.

The two physical descriptions of the probability of loop formation by the apoC-II fibrils both adequately describe at least some characteristics of the data and both provide insight into the loop formation process. The random walk description has the advantage of simplicity and transparency, and can be employed to explore the effects of fibril stiffness on loop assembly. It cannot, however, be extended to examine more subtle physical factors. The more sophisticated but computer-intensive model of loop formation as wormlike chains adequately describes the behavior at moderate length scales, and allows examination of the influence of less obvious physical parameters (including twist repeat length and end chirality) on the formation of loops. However, in the modeling of these finer physical constraints, the possible generation of unrealistic structures must be taken into consideration, requiring rigorous and detailed comparison with the increasingly sophisticated experimental methods that are now becoming possible for characterization of complex materials such as amyloid fibrils.

Other fibril systems

Given that our results suggest a general mechanism of end-to-end annealing which might be responsible for loop formation of apoC-II amyloid fibrils, it is of interest to consider the possibility of their existence in other amyloid systems. Transiently stable rings have been observed in early fibrillar species formed by α-synuclein, a protein associated with Parkinson's disease (Conway et al., 2000). These structures have contour lengths of ~100–300 nm, and based on their morphology, appear to have a similar degree of flexibility to apoC-II amyloid ribbons. Most amyloid

structures, on the other hand, have a more complex fibril architecture and consequently are significantly more rigid than apoC-II fibrils. It is clear that the probability of loop formation will be significantly lowered for fibrils of longer persistence length. Loop closure may also be dependent on other factors including number of β-sheets, the tendency of fibrils to repel or associate, and intrinsic nonrandom bending of fibrils.

Since closed loops cannot further polymerize, and if it is assumed they do not fragment, they act as a kinetic endpoint in the polymerization reaction. This has implications for conditions such as Parkinson's disease where small oligomeric aggregates or the small ring structures of α-synuclein amyloid fibrils have been suggested to be the more neurotoxic amyloid species in Lewy bodies (Conway et al., 2000). Events that promote the formation of small amyloid rings may therefore promote the stable formation of these potentially toxic species. This possibility is of particular significance because of the determination that the initially formed aggregates in systems that ultimately form amyloid fibrils may in general be toxic to cells (Bucciantini et al., 2002). It is also interesting to note that apoC-II and α-synuclein share many apolipoproteinlike properties, including the presence of amphipathic α-helical domains, existing in a natively unfolded state in solution, and binding to lipid in an α-helical conformation. The ability to allow loop closure of these two amyloid fibril-forming proteins may also lie in these shared properties.

The formation of closed loops by apoC-II also highlights the wide variety of structural morphologies available to amyloid fibrils. Despite the equivalence dictated by the invariant β-sheet core structure, amyloid fibrils are nonetheless capable of adopting a wide range of structures ranging from flexible ribbons through to rigid, rodlike arrays, all of which show great variation in diameter between species. This structural plasticity is dictated by sequence, and only by understanding these relationships will we be able to generate structures to-order, whereby the polypeptide precursor is used to define the morphology and physical properties of novel materials with potential practical utility (MacPhee and Dobson, 2001).

CONCLUSION

Amyloid fibrils constitute an alternative protein conformation to the biological fold that appears to be accessible to all, or at least many, peptide sequences under appropriate conditions. Despite a common core of cross-β-structure, amyloid fibrils from different proteins display remarkably different higher order structures giving rise to a range of morphologies. We have examined in detail the structure of the amyloid fibrils formed by human apolipoprotein C-II. These fibrils have a simple and homogeneous morphology, lacking the superstructural heterogeneity usually observed in amyloid species and arising from the aggregation of

protofilaments. This structural simplicity, and the determination of the apparent flexibility and dimensions of the fibrils, has allowed the development of simple models of the solution behavior of apoC-II amyloid fibrils. Such models, particularly when developed in greater detail, may be of general utility in elucidation of mechanisms of fibril formation and further characterization of fibril structural properties. Our results indicate that the presence of these loops and their observed size distribution can be explained by two simple models of loop formation in which the inherent flexibility of fibrillar apoC-II allows fibrils of appropriate length to bend back on themselves and anneal end-to-end to form a loop.

REFERENCES

Aggeli, A., M. Bell, N. Boden, J. N. Keen, T. C. B. McLeish, I. Nyrova, S. E. Radford, and A. Semenov. 1997. Engineering of peptide β-sheet nanotapes. *J. Mater. Chem.* 7:1135–1145.

Bucciantini, M., E. Giannoni, F. Chiti, F. Baroni, L. Formigli, J. Zurdo, N. Taddei, G. Ramponi, C. M. Dobson, and M. Stefani. 2002. Inherent toxicity of aggregates implies a common mechanism for protein misfolding diseases. *Nature.* 416:507–511.

Bonar, L., A. S. Cohen, and M. M. Skinner. 1969. Characterization of the amyloid fibril as a cross-β protein. *Proc. Soc. Exp. Biol. Med.* 131: 1373–1375.

Chamberlain, A. K., C. E. MacPhee, J. Zurdo, L. A. Morozova-Roche, H. A. Hill, C. M. Dobson, and J. J. Davis. 2000. Ultrastructural organization of amyloid fibrils by atomic force microscopy. *Biophys. J.* 79: 3282–3293.

Come, J. H., P. E. Fraser, and P. T. Lansbury, Jr. 1993. A kinetic model for amyloid formation in the prion diseases: importance of seeding. *Proc. Natl. Acad. Sci. USA.* 90:5959–5963.

Conway, K. A., S.-J. Lee, J.-C. Rochet, T. T. Ding, R. E. Williamson, and P. T. Lansbury, Jr. 2000. Acceleration of oligomerization, not fibrillization, is a shared property of both a-synuclein mutations linked to early-onset Parkinson's disease: implications for pathogenesis and therapy. *Proc. Natl. Acad. Sci. USA.* 97:571–576.

De Gennes, P. G. 1985. Scaling Concepts in Polymer Physics. Cornell University Press, Ithaca, NY.

Doi, M., and S. F. Edwards. 1986. The Theory of Polymer Dynamics. Oxford Press, Oxford, UK.

Fandrich, M., M. A. Fletcher, and C. M. Dobson. 2001. Amyloid fibrils from muscle myoglobin. *Nature.* 410:165–166.

Ferrone, F. 1999. Analysis of protein aggregation kinetics. *Methods Enzymol.* 309:256–274.

Goldsbury, C. S., G. J. Cooper, K. N. Goldie, S. A. Muller, E. L. Saafi, W. T. Gruijters, M. P. Misur, A. Engel, U. Aebi, and J. Kistler. 1997. Polymorphic fibrillar assembly of human amylin. *J. Struct. Biol.* 119: 17–27.

Gosal, W. S., A. H. Clark, P. D. A. Pudney, and S. B. Ross-Murphy. 2002. Novel amyloid fibrillar networks derived from a globular protein: β-lactoglobulin. *Langmuir.* 18:7174–7181.

Hatters, D. M., C. E. MacPhee, L. J. Lawrence, W. H. Sawyer, and G. J. Howlett. 2000. Human apolipoprotein C–II forms twisted amyloid ribbons and closed loops. *Biochemistry.* 39:8276–8283.

Hatters, D. M., R. A. Lindner, J. A. Carver, and G. J. Howlett. 2001. The molecular chaperone, crystallin, inhibits amyloid formation by apolipoprotein C–II. *J. Biol. Chem.* 276:33755–33761.

Jacobson, H., and W. H. Stockmayer. 1950. Intramolecular reaction in polycondensations. I. The theory of linear systems. *J. Chem. Phys.* 18: 1600–1606.

Jimenez, J. L., J. I. Guijarro, E. Orlova, J. Zurdo, C. M. Dobson, M. Sunde, and H. R. Saibil. 1999. Cryo-electron microscopy structure of an SH3 amyloid fibril and model of the molecular packing. *EMBO J.* 18: 815–821.

Kahn, J. D., and D. M. Crothers. 1998. Measurement of the DNA bend angle induced by the catabolite activator protein using Monte Carlo simulation of cyclization kinetics. *J. Mol. Biol.* 276:287–309.

Levene, S. D., and D. M. Crothers. 1986. Ring closure probabilities for DNA fragments by Monte Carlo simulation. *J. Mol. Biol.* 189:61–72.

Lomakin, A., D. B. Teplow, D. A. Kirschner, and G. B. Benedek. 1997. Kinetic theory of fibrillogenesis of amyloid β-protein. *Proc. Natl. Acad. Sci. USA.* 94:7942–7947.

MacPhee, C. E., and C. M. Dobson. 2001. Formation of mixed fibrils demonstrates the generic nature and potential utility of amyloid nanostructures. *J. Am. Chem. Soc.* 122:12707–12713.

MacRaild, C. A., D. M. Hatters, L. J. Lawrence, and G. J. Howlett. 2003. Sedimentation velocity analysis of flexible macromolecules: self-association and tangling of amyloid fibrils. *Biophys. J.* 84:2562–2569.

Mandelkow, E., and K. C. Holmes. 1974. The positions of the N-terminus and residue 68 in tobacco mosaic virus. *J. Mol. Biol.* 87:265–273.

Naiki, H., and K. Nakakuki. 1996. First-order kinetic model of Alzheimer's β-amyloid fibril extension in vitro. *Lab. Invest.* 74:374–383.

Parker, M. W., J. T. Buckley, J. P. Postma, A. D. Tucker, K. Leonard, F. Pattus, and D. Tsernoglou. 1994. Structure of the *Aeromonas* toxin proaerolysin in its water-soluble and membrane-channel states. *Nature.* 367:292–295.

Petkova, A. T., Y. Ishii, J. J. Balbach, O. N. Antzutkin, R. D. Leapman, F. Delaglio, and R. Tycko. 2002. A structural model for Alzheimer's β-amyloid fibrils based on experimental constraints from solid state NMR. *Proc. Natl. Acad. Sci. USA.* 99:16742–16747.

Pham, C. L. L., D. M. Hatters, L. J. Lawrence, and G. J. Howlett. 2002. Cross-linking and amyloid formation by N- and C-terminal cysteine derivatives of human apolipoprotein C–II. *Biochemistry.* 41:14313–14322.

Rivetti, C., M. Guthold, and C. Bustamante. 1996. Scanning force microscopy of DNA deposited onto mica: equilibration versus kinetic trapping studied by polymer chain analysis. *J. Mol. Biol.* 264:919–932.

Rochet, J. C., K. A. Conway, and P. T. Lansbury, Jr. 2000. Inhibition of fibrillization and accumulation of prefibrillar oligomers in mixtures of human and mouse a-synuclein. *Biochemistry.* 39:10619–10626.

Schagger, H., and G. von Jagow. 1987. Tricine-sodium dodecyl sulfate-polyacrylamide gel electrophoresis for the separation of proteins in the range from 1 to 100 kDa. *Anal. Biochem.* 166:368–379.

Serpell, L. C. 2000. Alzheimer's amyloid fibrils: structure and assembly. *Biochim. Biophys. Acta.* 1502:16–30.

Serpell, L. C., M. Sunde, M. D. Benson, G. A. Tennent, M. B. Pepys, and P. E. Fraser. 2000. The protofilament substructure of amyloid fibrils. *J. Mol. Biol.* 300:1033–1039.

Serpell, L. C., P. E. Fraser, and M. Sunde. 1999. X-ray fiber diffraction of amyloid fibrils. *Methods Enzymol.* 309:526–536.

Sipe, J. D., and A. S. Cohen. 2000. History of the amyloid fibril. *J. Struct. Biol.* 130:88–98.

Tjernberg, L. O., D. J. Callaway, A. Tjernberg, S. Hahne, C. Lillíehook, L. Terenius, J. Thyberg, and C. Nordstedt. 1999. A molecular model of Alzheimer amyloid beta-peptide fibril formation. *J. Biol. Chem.* 274: 12619–12625.

Wang, C. S., D. Downs, A. Dashti, and K. W. Jackson. 1996. Isolation and characterization of recombinant human apolipoprotein C–II expressed in *Escherichia coli. Biochim. Biophys. Acta.* 1302:224–230.